VOLT: The Victoria Open Loop Testbed

David R. Andersen*[a], Michael Fischer[a], Rodolphe Conan[b], Murray Fletcher[a], and Jean-Pierre Véran[a]
[a]NRC Herzberg Institute of Astrophysics, 5071 W. Saanich Rd, Victoria, BC, Canada V9E 2E7;
[b]University of Victoria, PO Box 3055 STN CSC, Victoria, BC Canada V8W 3P6

ABSTRACT

The Victoria Open Loop Testbed (VOLT) serves as a demonstration of open loop control both on-sky (at the Dominion Astrophysical Observatory's 1.2m telescope) and in the lab in order to facilitate the future development of Multi-Object Adaptive Optics (MOAO). MOAO, when combined with multiple deployable integral field units, is a concept which promises to deliver near diffraction-limited images over a large field of view. Astronomers will be able to use the multiplex advantage of MOAO instruments to mount large, detailed surveys of galaxies and star formation regions. However, several challenges await MOAO instrument designers. The greatest of these is implementing open loop control in an astronomical adaptive optics (AO) system. Almost all astronomical AO systems to date have used some form of closed loop control, in which the wavefront sensors (WFSs) measure a residual wavefront error after the deformable mirror (DM) has taken on its commanded shape. WFSs in an open loop system can be spatially separated from the DM, but doing so creates new challenges, some known and some unknown. Uncertainties springing from open loop control pose the greatest risk to the design of a MOAO instrument. To mitigate this risk, we have designed and built VOLT, a simple on-axis open loop adaptive optics system. We describe several sources of open loop error, and our measurements of their expected contribution to the VOLT performance. Finally we present observations of a bright star, showing that VOLT, operating in open loop, was able to significantly improve the image quality from 2.5 arcseconds to 0.5 arcseconds in I-band, consistent with our estimates of the wavefront errors. We also present the open loop rejection transfer function for VOLT based on both on-sky and lab measurements.

Keywords: Adaptive Optics, Open Loop Control**,** Laboratory Testbed

1. INTRODUCTION

Multi-Object Adaptive Optics (MOAO) is a novel AO approach to the problem of achieving diffraction-limited images within very large fields of regard using ground-based telescopes[1-3]. Deployable integral field units (IFUs), each containing a deformable mirror (DM), can be incorporated into an instrument with a 10-40 times multiplex advantage over a single, on-axis IFU behind a more traditional AO system[4]. Before MOAO systems are incorporated into instruments for 8 to 30m telescopes, however, there are several risks that need to be retired. Many of the challenges involved in designing a MOAO system, such as the use of tomography, MEMS mirrors, and woofer-tweeter control, have all been demonstrated to work in different lab settings and are included in advanced instrument concepts. Open loop control (Figure 1), however, is perhaps the greatest risk to MOAO, partly because it is the biggest unknown. While open loop control is not a new idea (Primmerman et al. used so-called "go to" adaptive optics to make corrections and take science images immediately following pulses from a laser guide star with a low duty cycle[5]), interest in implementing open loop control on sky has been re-invigorated in the past few years[6-10]. After all, open loop control introduces unique requirements on an AO system: The WFS needs to have a high dynamic range; DM hysteresis and non-linearity need to be mitigated; Finally, alignment and calibration become more challenging.

We have built VOLT (the Victoria Open Loop Testbed) to try to distill the problems associated with open loop control from other challenges facing the design of a MOAO system and demonstrate the concept on-sky. VOLT is a simple, on-axis natural guide star AO testbed deployed at the Coudé focus of the Dominion Astrophysical Observatory (DAO) 1.2m telescope. There, we have the benefit of a thermally isolated, gravitationally constant environment for our instrument.

* david.andersen@nrc-cnrc.gc.ca; phone 1 250 363-8708; fax 1 250 363-0045

Adaptive Optics Systems, edited by Norbert Hubin, Claire E. Max, Peter L. Wizinowich,
Proc. of SPIE Vol. 7015, 70150H, (2008)
0277-786X/08/$18 · doi: 10.1117/12.789792

Still DAO offers challenges, as the expected D/r_0 values are typically 20-30. In these proceedings, we will describe the VOLT design, and then look into a few of the wavefront error terms associated with open loop control. We will then present our first on-sky results with VOLT, and compare our results to simulations of VOLT and to our lab and calibration measurements. Finally, we will conclude with a description of the current status and the future plans for VOLT.

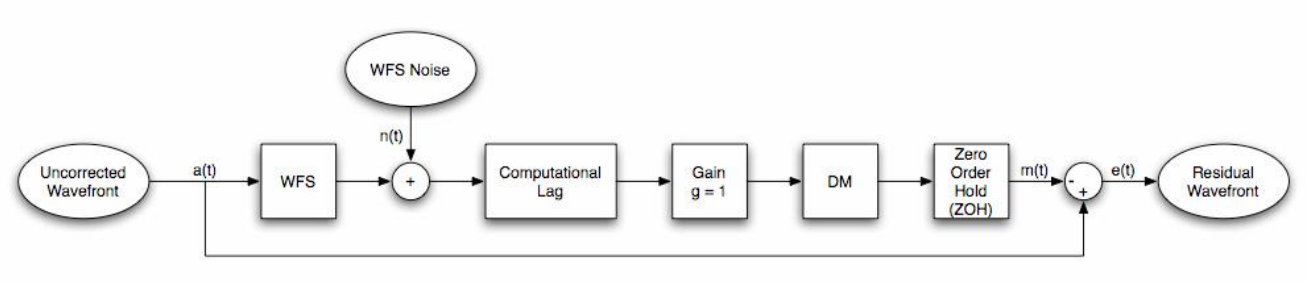

Figure 1: In the most basic implementation of an open loop control architecture, the slopes measured by the WFS are directly converted into DM commands using the reconstructor and a gain of 1. Unlike in a closed loop AO system, no integrator is required.

2. DESIGN

In this section, we will describe the architecture of VOLT. The VOLT system consists of a set of passive optics and sensors and active hardware components, as well as two control computers with specialized interface cards. The layout of the optics and cameras are shown in Figure 2 while the interconnections between the active components are shown in Figure 3. The description of the VOLT optics begins with a consideration of the telescope itself; the DAO 48-inch telescope is 1.2m in diameter with a ~0.2m secondary mirror (central obscuration). The image scale at telescope focus is 4.88 arcsecond/mm (f/34.6). The entrance aperture at the telescope focus is 8 arcseconds in diameter (1.64 mm). A fold mirror cantilevered off the VOLT optical bench picks off the light after focus inside the Coudé room and redirects the light into the VOLT instrument.

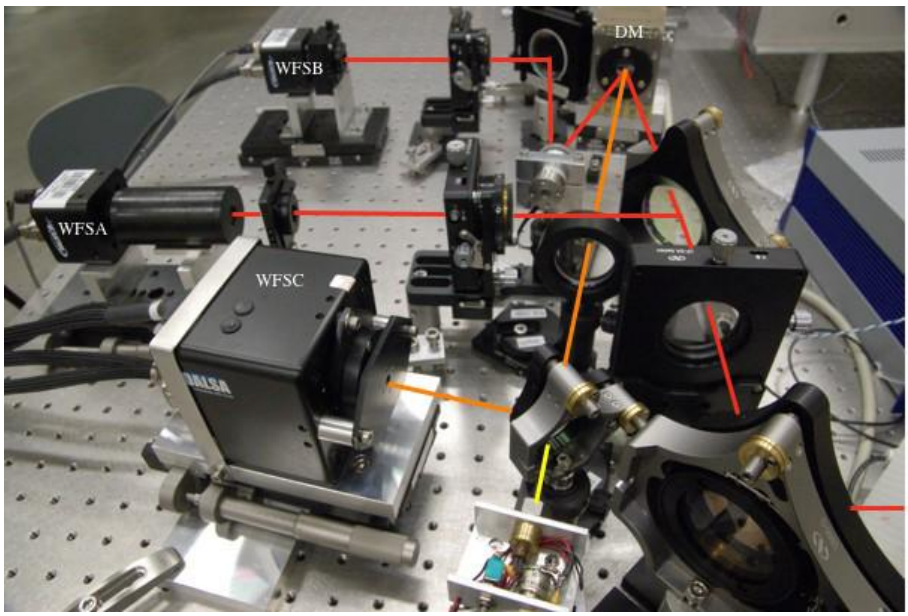

Figure 2: Photograph of the VOLT optical layout, with lines illustrating the optical path. After the pick-off mirror and the collimator, a beamsplitter directs light into the open loop WFS arm of VOLT (WFS A). The light that passes through the beamsplitter encounters the DM, another fold mirror and a second beamsplitter which divides the light between the scoring WFS (WFS B) and the science camera. The science camera is not pictured. A truth WFS (WFS C) has an independent optical path with its own light source. WFS C can be used to monitor the DM shape.

After the light is collimated, a beamsplitter directs 70% of the light into wavefront sensor (WFS) A, the open loop WFS. The WFS A optics consist of two lenses and a field stop that re-collimate a 7.6 arcsecond field of view (FOV) beam onto 7x7 elements of the AOA768-86-S lenslet array. All three WFSs in VOLT are 7x7 subaperture Shack-Hartmann WFSs, with the edges and central subaperture removed, leaving 36 valid lenslets. A final lens re-images the spots onto a Dalsa 1M150 CMOS detector with a pixelscale of 0.485 arcsec/pixel and 16 pixels/subaperature. The 1M150 is a 1024 x 1024 array of 10.6µm pixels, of which we only read out a 160x160 pixel subregion. Subregion readout allows running the camera at the ~1kHz frame rate required for the open-loop experiment. The 1M150 frame capture is controlled via a CameraLink interface to an EDT PCI DV C-Link framegrabber board on control PC 1.

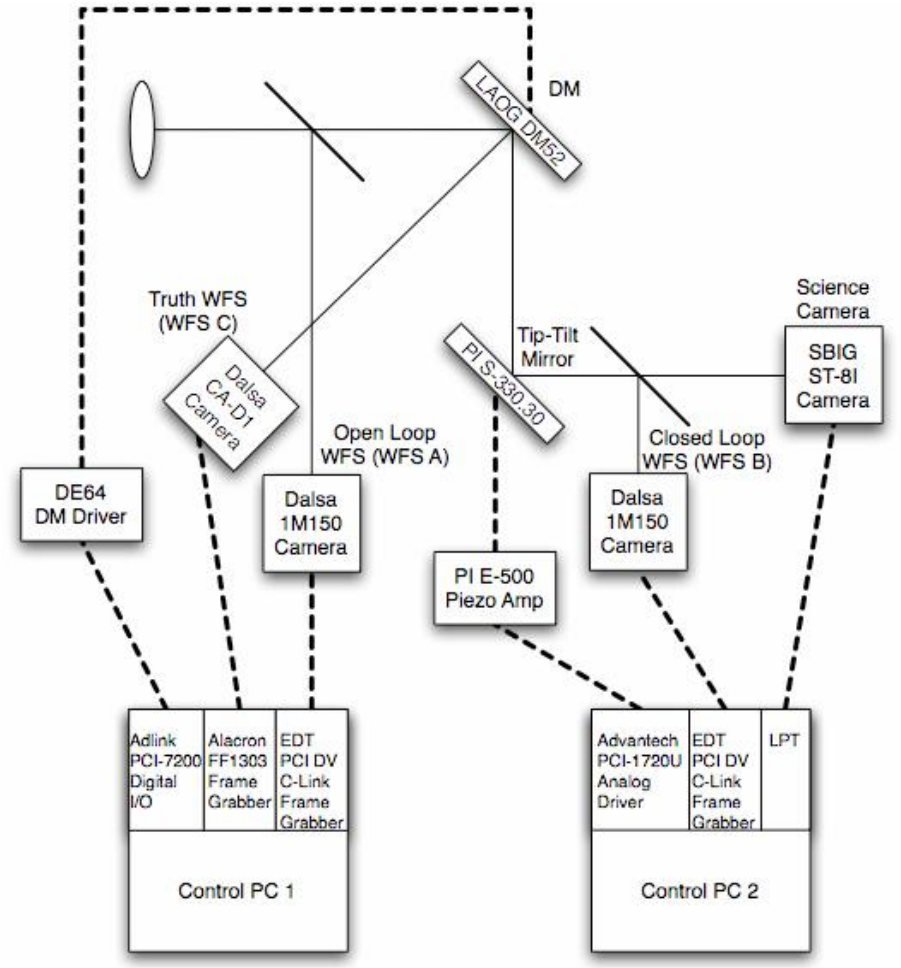

Figure 3: The system architecture of VOLT highlighting the interconnections between the control PCs, the specialized PCI cards, and the active hardware.

After the first VOLT beamsplitter, the beam encounters the Laboratoire Astrophysique de l'Observatoire de Grenoble (LAOG) ALPAO DM52, a 52 voice-coil actuator (arranged on an 8x8 rectangular grid) deformable mirror with a 17.6mm diameter pupil and actuator spacing (pitch) of 2.5mm. Important characteristics that make it suitable for open-loop operation are its large wavefront stroke (up to 25µm), very smooth influence functions and high linearity with no hysteresis. It is driven by the LAOG ALPAO DE64 drive electronics, a 64 channel amplifier commanded by a parallel digital interface. To satisfy the 1kHz mirror update rate required by VOLT, a high speed Adlink PCI-7200 digital I/O board is used to send DM commands from Control PC 1 to the DE64. In order to best utilize the surface of the DM, we wish to minimize the incident beam angle. The incident beam angle is 11.01 deg (the cosine of which is 0.982). The telescope exit pupil is imaged on the DM.

After another reflection, the beam encounters the second beamsplitter. Here most of the remaining light is directed into WFS B. WFS B can be used with the DM in traditional closed loop operation, but we primarily use WFS B to register

WFS A to the DM and to measure the residual wavefront errors in open loop operation. The optics again consist of two lenses and pinhole which re-collimates a 3.9 arcsecond beam onto a AOA 250-17-S lenslet array. The images from this lenslet array are recorded by a second Dalsa 1M150 detector interfaced to Control PC 2 via another EDT framegrabber. Each 19x19 pixel subaperture has a platescale of 0.15 arcseconds/pixel.

Following the other channel of the second beamsplitter, a lens focuses the image onto the science detector, a SBIG ST-8I CCD camera. It has a detector array of 1530x1020 9μm pixels, of which a 152x152 subregion is read out to display the corrected science images. The science camera has a platescale of 0.053 arcseconds/pixel which should place three pixels across the FWHM of a 900nm diffraction-limited image from the 1.2m telescope. The ST-8I is a relatively old camera and is connected to its host computer via the parallel printer port, however its readout rate is not required to be high but only needs to provide a relatively continuous visual display of the system image correction for the user.

We have a separate optical path in VOLT to accommodate a truth WFS, WFS C. WFS C provides an absolute reference of the DM shape. We can repeatably remove the DM and replace it with a reference flat mirror, and thereby determine the voltages required to have the DM take on a flat shape. Light from a LED source is collimated and directed at the DM face-on. On the return path, a fraction of the light is picked off by a beamsplitter and directed through the WFS optics, which consists of a re-collimator and an AOA 190-11-S array. The spots are directly imaged by a DALSA CAD-1 128x128 CCD detector with 16μm pixels. It is connected to its host computer by a RS422 interface provided by an Alacron FastFrame 1303 PCI framegrabber board (FF1303) and can be read out at 700Hz. Each subaperture is 12 pixels across and has an equivalent image scale of 0.22 arcseconds/pixel.

The VOLT system is controlled by two desktop PCs running an installation of Linux optimized for real-time performance with the framegrabber, digital I/O, and analog driver cards as shown in Figure 3 and described in the preceding sections. Control PC 1 is a 1.8GHz machine and handles the open-loop real-time control and DM surface shape monitoring. The remaining closed loop functionality and science camera image capture is handled by Control PC 2, a 1.5GHz machine. The open loop real-time control timing is shown in Figure 4. A loop iteration begins with the DMA transfer of a completed WFSA frame from the camera to the host via the EDT framegrabber. Once the frame is transferred, the WFSA camera is triggered to begin exposure of the next frame and centroid computation is performed on the frame just captured. Computed centroids are then used to generate new DM commands after a reconstructor-matrix-by-centroids-vector multiplication, the result of which is dispatched by DMA to the PCI-7200 DM driver board to carry out the high-speed writing of DM actuator voltage values to the DE64 amplifier. The remainder of the loop iteration is idle time spent waiting for the next WFS camera exposure to complete (depending on the particular exposure time).

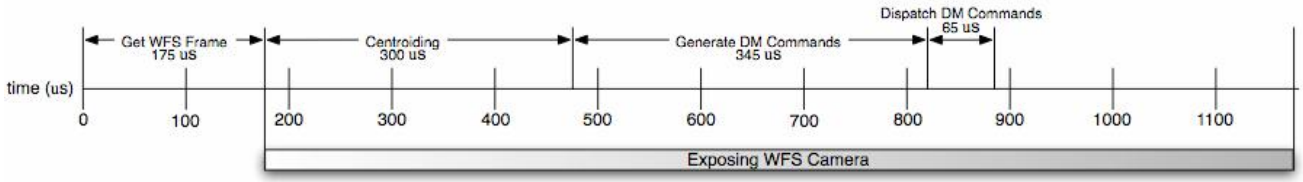

Figure 4: Timing diagram for a single iteration of the open-loop real-time controller for a 1 ms WFS exposure time, giving a control loop bandwidth in this case of 850Hz.

3. OPEN LOOP WAVEFRONT ERRORS

There are a number of potential wavefront error sources that are especially important in open loop AO systems. DM non-linearities and hysteresis are two such sources because in an open loop AO system, they are just non-common path wavefront errors. Therefore, we studied go-to characteristics of the ALPAO DM in the early phases of the VOLT project. We used a WYKO interferometer to measure the response of the DM from each actuator. Once we had mapped out the influence functions, we projected realistic turbulence maps onto the basis of influence functions in order to generate the optimal shape of the DM in response to that turbulent phase screen and then commanded the mirror to take on that optimal shape in a single step (gain=1; Figure 5). The difference between the optimal shape and the measured shape of the mirror is an open loop error due to both DM hysteresis and non-linearities but was quite small, just ~10nm for the ALPAO DM – roughly five times smaller than the fitting error (Figure 6).

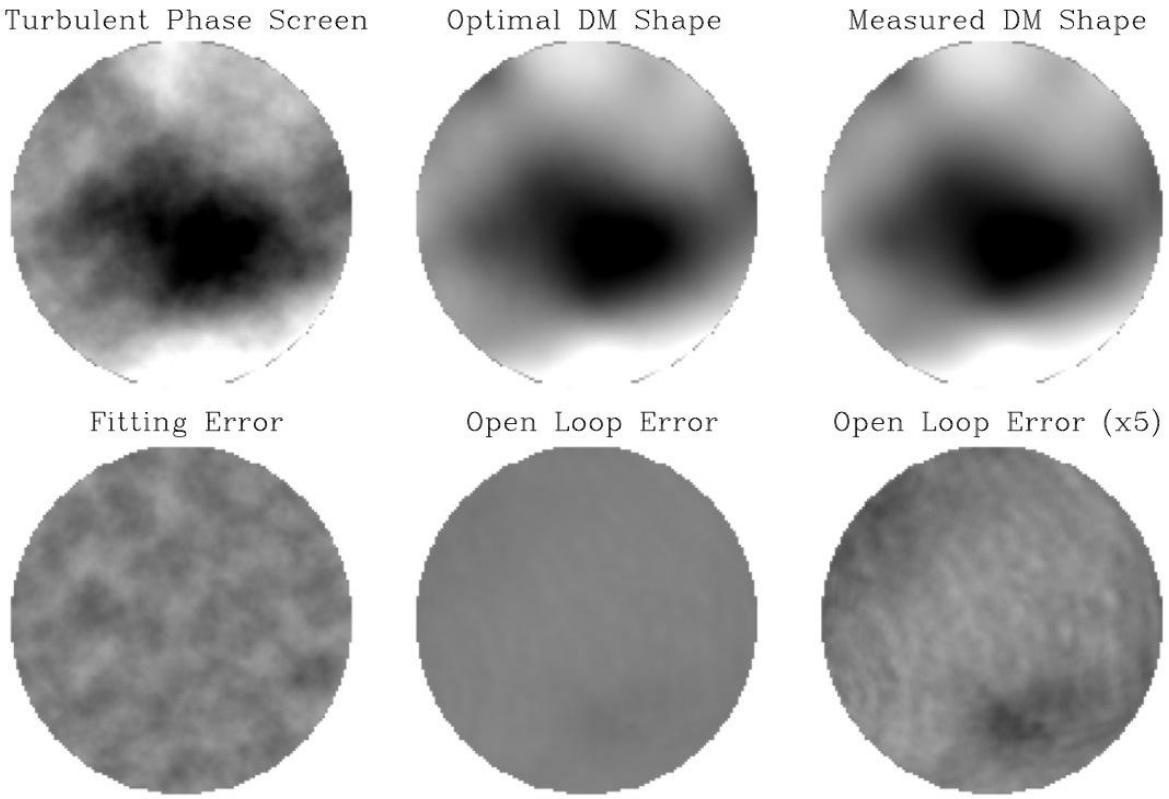

Figure 5: Top Left: Simulated phase screen corresponding to r_0=5cm on a 1.2m telescope. Top center: By projecting the ALPAO DM influence functions onto simulated phase screens, we could determine the optimal shape of the DM and generate the appropriate DM commands. Top Right: After applying the appropriate voltages to the DM, we measured the shape of the DM with the interferometer. Bottom Left: The difference between the phase screen and the optimal DM shape is the fitting error. Bottom Center and Bottom Right: The difference between the optimal and measured DM shapes is an open loop error. For the ALPAO DM, it is roughly five times smaller than the fitting error.

After establishing that the ALPAO DM is well-suited for use in an open loop AO system, we integrated the DM into the VOLT system. Key to the operation of any open loop AO system is the ability to register the open loop WFS to the DM. We take advantage of WFS B and a LED calibration source to achieve this registration. We adjust the WFS B optics so that the location of the DM actuators fall on the corners of four subapertures. We then generate the WFS B interaction matrix by measuring the location of each Shack-Hartmann spot in response to the movements of each DM actuator. The closed loop reconstructor is just the inverse of this interaction matrix. We then register WFS A to WFS B. We begin this process by placing masks just after the VOLT collimator which illuminate only a few subapertures on WFS B. We then adjust the WFS A optics to produce the same illumination pattern on WFS A. Once the two WFSs appear well-registered, we confirm and quantify the registration by placing phase screens in the beam just after the collimator. By comparing the centroids measured on both WFS A and B, we can determine the relative plate scales of the two WFSs (We measure the absolute plate scale of WFS A by rotating a plate through a known angle which produces a known offset in arcseconds). The WFS A reconstructor is then created by scaling the WFS B reconstructor by the ratio of the platescales. We measure the rms scatter in the relation between the WFS A and B plate scales of just 0.06 arcseconds (Figure 7), which corresponds to a registration wavefront error of 70nm.

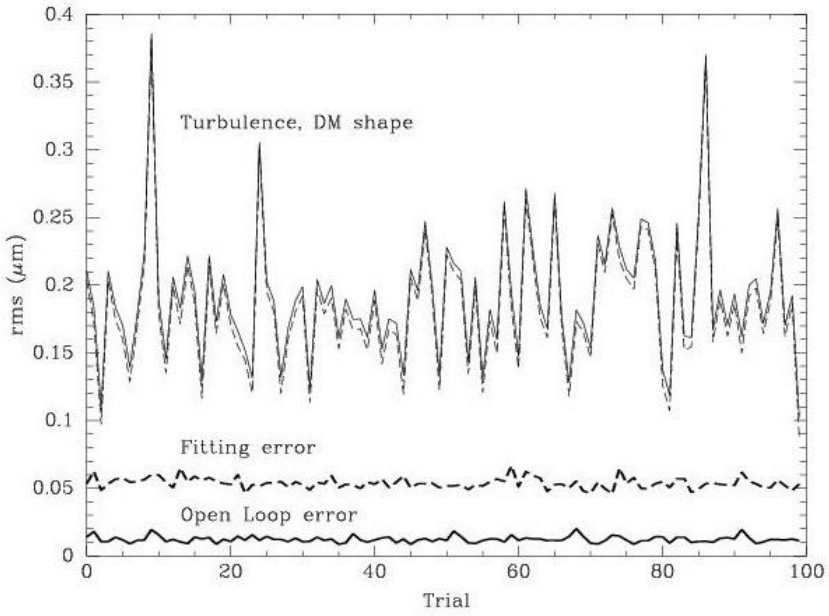

Figure 6: Plot of the standard deviation of the wavefront variations of the simulated phase screens (thin solid line) and the DM shape (thin dashed line) for 100 different realizations of D/r_0=25 turbulence. For each realization, we also calculated the fitting error (~50nm; thick dashed line) and the open loop error (just ~10nm; thick solid line).

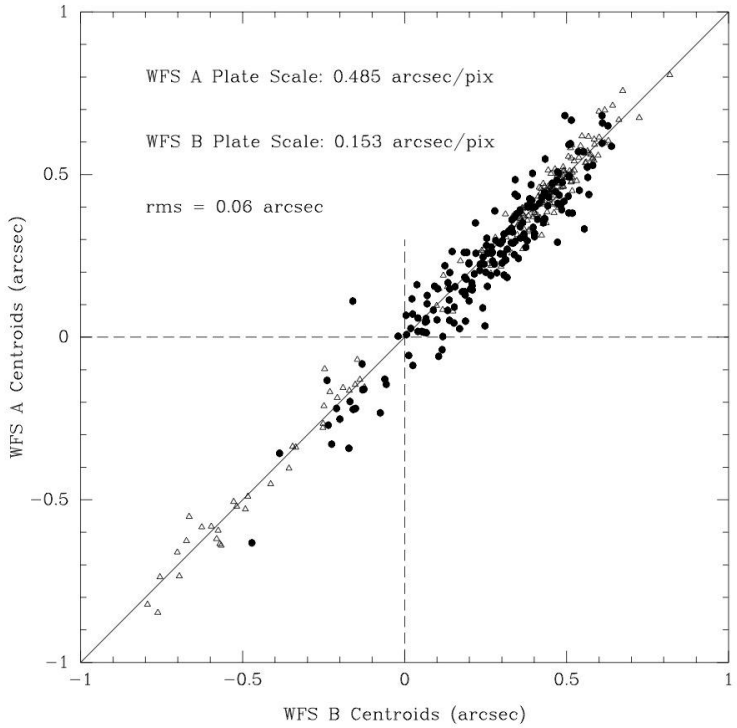

Figure 7: Vertical (filled circles) and Horizontal (open triangles) slopes measured on WFS A and WFS B. The standard deviation of the slopes around a unity slope is 0.06 arcseconds, which translates into a registration error of just 70nm.

Once WFS A and WFS B are aligned and we have built the WFS A reconstructor, VOLT can apply open loop corrections. We initially test that VOLT is working by correcting aberrations from static phase screens in single steps. After establishing that the resultant corrected images are still diffraction-limited, we can align VOLT to the telescope and prepare to observe.

4. ON SKY RESULTS

On May 22nd, 2008, we had our first success applying an open loop correction on-sky. The night was clear, but the seeing was poor; we measured the FWHM of Arcturus (R=0.3[11]) to be 2.5 arcseconds in I-band which corresponds to an r_0=4cm at 500nm. After aligning Arcturus on WFS A and WFS B, we were able to operate VOLT in open loop with a sampling frequency of 750Hz on WFS A. Less than half the light that arrives at WFS A is available at WFS B due to the 70/30 beamsplitter. Furthermore, the light is spread out over 10 times more pixels on WFS B, so we were only able to use a sampling frequency of 50Hz for WFS B. Even at these sampling frequencies, we were operating in a very low S/N regime; our centroiding algorithm is a simple moment measurement with thresholding. The presence of substantial pattern noise on the 1M150 detectors forced us to raise our threshold a factor of 6 greater than the readnoise. The peak flux above that threshold was just a factor of 3-5 greater, so we were introducing substantial WFS noise. By using our calibration source to match the relatively low light-levels of Arcturus, we were able to estimate that the contribution to the VOLT error budget due to WFS A noise was between 250nm and 500nm (we adopt 300nm here). The next greatest VOLT wavefront error term also had little to do with open loop operation; PAOLA[12] simulations indicated that we could expect another 200nm of wavefront error due to lag. The 70nm of non-common path error due to the misalignment of WFS A to WFS B and the DM is relatively inconsequential in comparison. The quadrature sum of all these terms (plus the 50nm of fitting error and 10nm of open loop "go-to" error; Figure 6) is 370nm. This estimate of the VOLT total wavefront error agrees qualitatively with the 0.5 arcsecond FWHM VOLT performance observed (Figures 8-9) and earlier CAOS[13] simulations of VOLT (Figure 10).

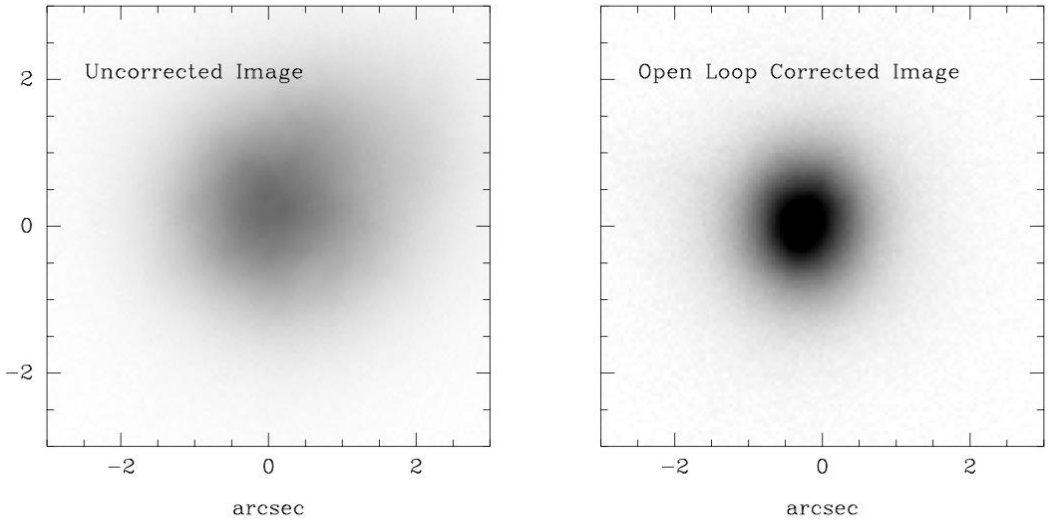

Figure 8: VOLT images of Arcturus from May 22, 2008. In the left panel, the I-band FWHM of the uncorrected image is 2.5arcseconds, which corresponds to 4cm at a wavelength of 500nm. With the open loop wavefront sensor taking frames at 750 Hz, we obtained significant image correction, with the FWHM dropping to 0.5 arcseconds. Both exposures were 20s, and both images have the same log stretch, demonstrating the factor of five increase in the peak flux.

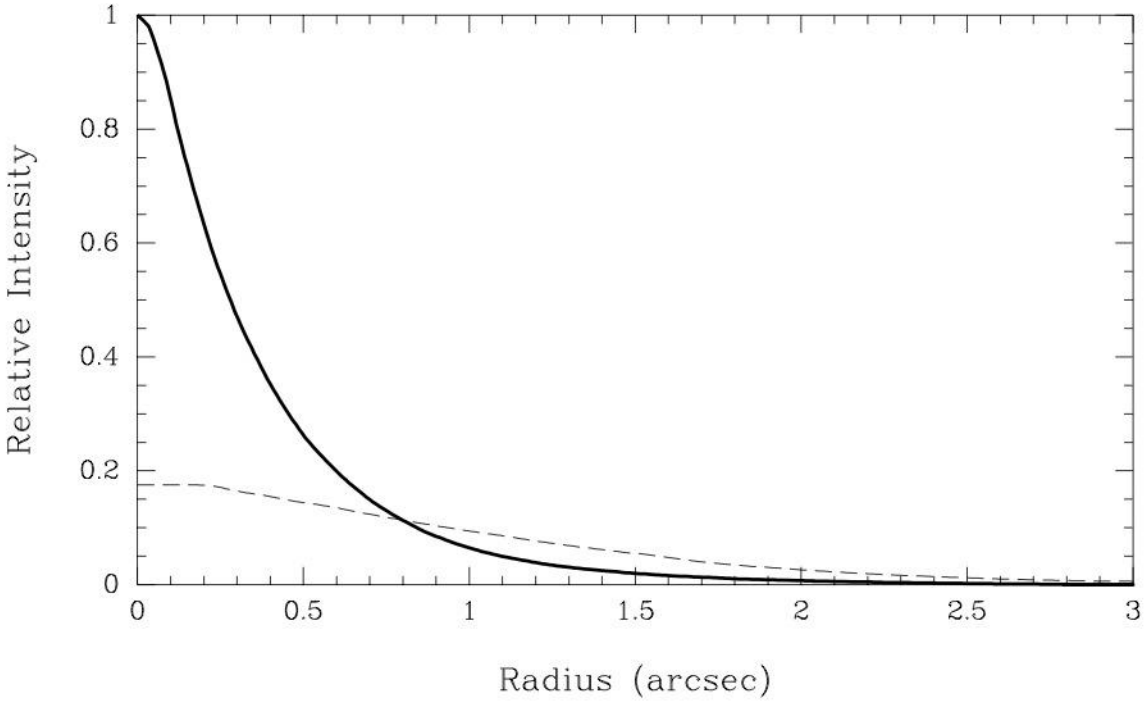

Figure 9: Radial profiles of the two images of Arcturus shown in Figure 8. The uncorrected image is shown with a dashed line, and the open loop corrected image is drawn with a heavy solid line. These profiles show the significant reduction in FWHM with the open loop correction applied (2.5 arcsecond to 0.5 arcsecond FWHM), and the factor of 5 increase in the peak flux. The level of correction observed is consistent with our lab measurements of the WFS noise error, which dominates the VOLT error budget.

While observing with VOLT, we store all centroids measured for WFS A and WFS B. We project these measurements onto low order Zernike polynomials in order to measure the power spectral density (PSD) of the turbulence and the residual correction (Figure 11). The power spectrum of the open loop measurements from WFS A show that the power of the measured turbulence was proportional to $f^{-2.64}$, where f is the frequency, as expected from theory ($f^{-8/3}$). At low temporal frequencies, we see that the residual PSD measured by WFS B is substantially lower (we are limited to measuring the VOLT correction to 25Hz because of the low S/N of spots measured on WFS B). If we take the ratio of these PSDs, we can show the open loop rejection transfer function (RTF) measured on-sky (Figure 12). Shown with the on-sky RTF is the lab-measured RTF. For the lab measurement, we used only measurements from WFS B. We took two time series of centroids with WFS B with and without the open loop correction being applied. We found, however, that we can not take these time series while the system runs only on WFS noise alone, as WFS A has substantially higher WFS noise than WFS B at high S/N (which again is a product of the much finer WFS B pixel scale). Therefore, we need to inject noise into the system that is substantially higher than the WFS A noise floor. We do this by blowing hot air through the beam during the measurements. Figure 12 shows that at low frequencies, the lab RTF measurement begins to level off, undoubtedly due to the higher noise floor of WFS A being translated into a decrease in perceived performance by WFS B. The on-sky RTF measurement is not subject to this effect because the amount of atmospheric turbulence is significantly greater than the turbulence source used for the lab measurements. The lab-measured RTF shows that at 750 Hz, we achieve some correction at frequencies less than 70Hz. The peak of the RTF is close to 6db and 187.5Hz ($F_s/4$), the expected overshoot of an open loop system with a simple controller (Figure 1). The slope of the RTF is 17db of rejection per decade in frequency, which is consistent with an open loop control system that has a delay slightly longer than one frame.

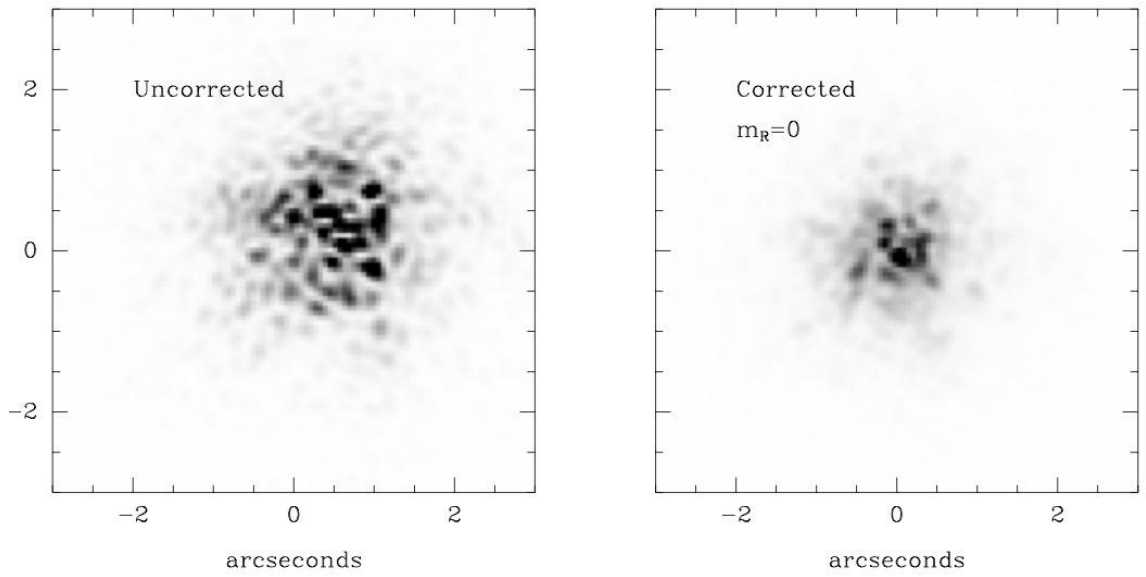

Figure 10: CAOS simulations of VOLT for a R=0 star (Arcturus has R=0.3) for r_0=4cm. These images are consistent with our observations of Arcturus (Figures 8-9). The FWHM measured from this image is 0.6 arcseconds.

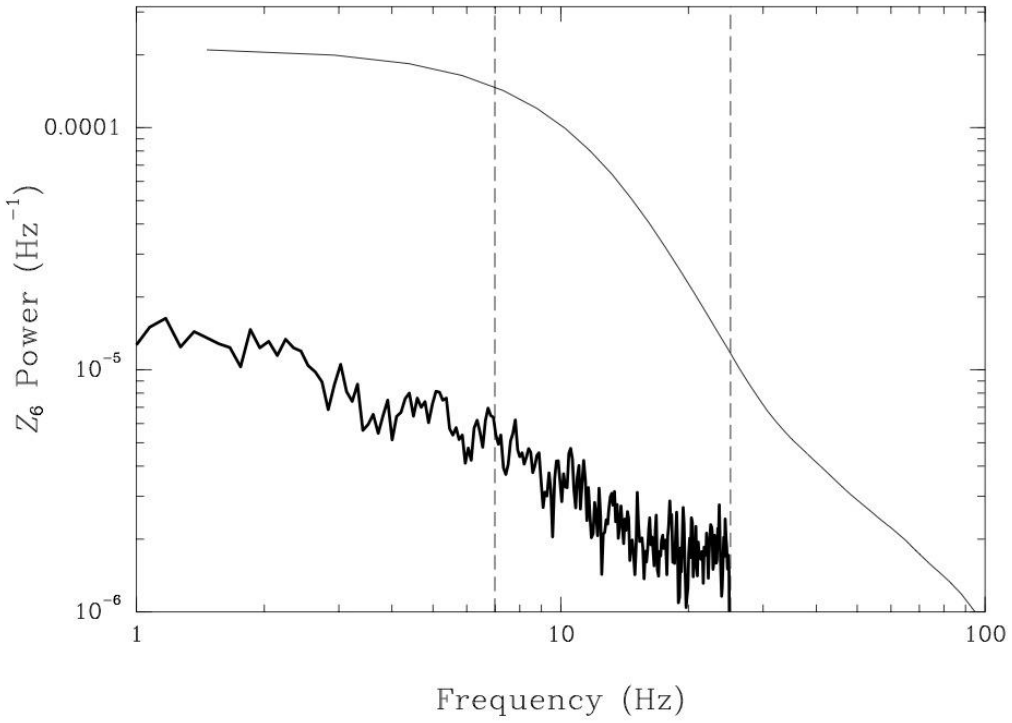

Figure 11: Relative power spectral densities of the atmosphere (measured by projecting the open loop WFS A centroids onto the sixth Zernike polynomial; thin solid line) and the open loop corrected wavefront (measured by projecting the open loop WFS B centroids onto the sixth Zernike polynomial; thick solid line). The maximum frequency to which we can measure the WFS B PSD is 25Hz, set by the signal to noise of the WFS spots on WFS B. The WFS A atmospheric PSD between the two dashed lines is proportional to $f^{-2.64}$, which is very close to $f^{-8/3}$ expected for Kolmogorov turbulence. The difference between the two curves shows that we are obtaining a significant open loop correction.

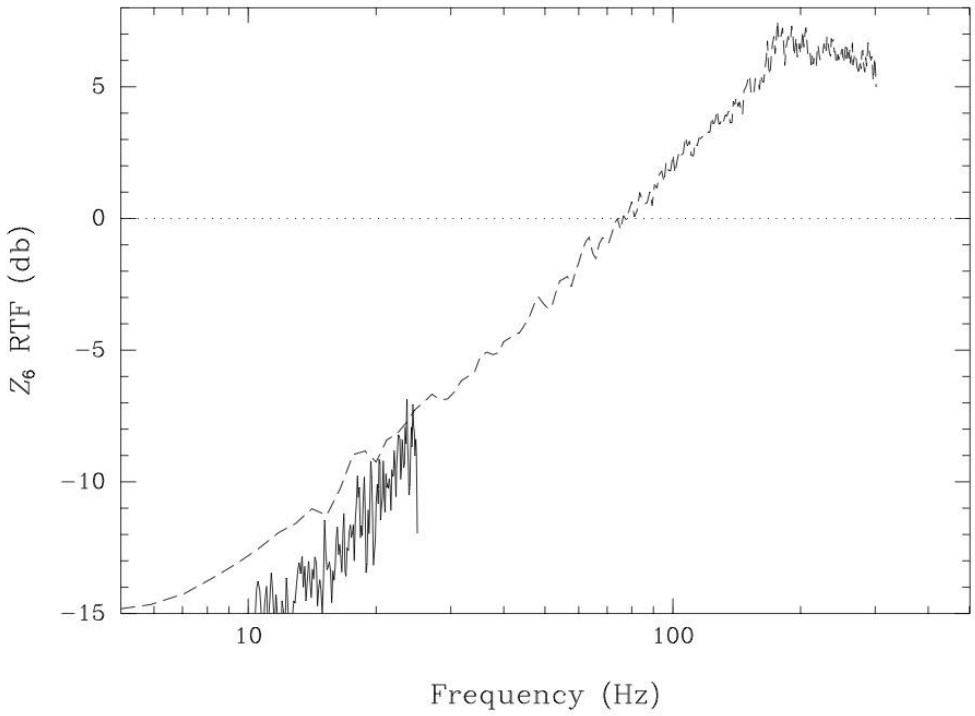

Figure 12: The rejection transfer function for the sixth Zernike Polynomial measured in the lab (dashed line) and on-sky from observations of Arcturus (solid line). By taking the ratio of the two PSDs between the dashed lines shown in Figure 11, we are able to measure the on-sky RTF of VOLT operating in open loop at 750Hz. There is very good agreement between this data and the lab-measured RTF. The lab measured RTF was obtained from time series of centroids measured just from WFS B with and without open loop correction. Because the WFS A noise is significantly larger than the WFS B noise in the limit of bright sources (the centroiding accuracy of WFS B is better because of the much finer pixel scale; Figure 7), we need to introduce some artificial turbulence into the beam during measurements to raise the signal above the noise floor. The PSD of the corrected WFS B time series at the lowest temporal frequencies may be approaching this noise floor. This may account for the decrease in rejection measured in the lab versus on-sky (where the atmospheric turbulence was much greater than the WFS noise floor). The lab-measured RTF does show the response of VOLT at higher temporal frequencies. The frequency corresponding to 0db of correction is 70Hz. The theoretical open loop RTF predicts a 6db overshoot which occurs at 187.5Hz ($F_s/4$), which agrees closely with these measurements.

5. SUMMARY

The goal of VOLT was to demonstrate open loop control on-sky and in the lab using a simple, on-axis natural guide star. The major components of the design are an ALPAO 52 actuator DM, an imaging CCD with a pixel scale sufficient to well sample a diffraction-limited image from the DAO 1.2m telescope, and three wavefront sensors tasked to sense: 1) the open-loop atmospheric turbulence (WFS A), 2) the residual wavefront error after the WFS A slopes are used to generate DM commands (WFS B), and 3) the DM shape using an independent light source (WFS C). Tests using an interferometer have shown that the "go-to" characteristics of the ALPAO mirror are excellent; repeated measurements of the DM shape relative to the optimal shape of a mirror responding to Kolmogorov turbulence with r_0=5cm indicate that the go-to error arising from DM hysteresis and non-linearities are ~10nm, a value much smaller than the fitting error (and other VOLT wavefront error terms). Another important open loop error term relates to the non-common path aberrations induced by a misregistration between the DM and the open loop wavefront sensor. We have described how we registered the open loop WFS A to the DM while introducing just an additional 70nm of wavefront error.

We were able to demonstrate open loop control on-sky on May 22, 2008. While observing Arcturus (R=0.3), we were able to obtain a substantial improvement in image quality (from 2.5 arcsecond FWHM to 0.5 arcsecond FWHM) while operating VOLT at a framerate of 750Hz using WFS A, consistent with simulations. We estimate that the residual

wavefront error after open loop correction was ~400nm, which is consistent with our measurements of WFS A noise (~300nm), lag (200nm), registration (70nm), fitting (50nm) and go-to (10nm) wavefront errors. We projected the centroids measured from WFS A and WFS B onto Zernike polynomials, and were able to show that the open loop WFS power spectrum of turbulence has a slope proportional to $f^{-2.64}$, very close to the expected slope of $f^{-8/3}$. Using the residual wavefront measurements of the scoring WFS B that were taken simultaneously, we were able to measure an on-sky RTF up to 25Hz. This section of RTF is in good agreement with the lab measured RTF. Overall, the lab-measured RTF meets our expectations based on analysis of the simple open loop controller.

Initially, we had hoped to achieve diffraction-limited performance for bright stars with VOLT, but after measuring the low telescope throughput (including 5 Aluminum mirrors) and the high 230e^- readnoise of the 1M150 WFS detectors, our expectation of the initial VOLT performance were lowered. Having achieved an open loop correction with VOLT, our new goal is to lower the lag and WFS noise wavefront error terms sufficiently to achieve diffraction-limited performance and be able to sense how changes in DM to WFS alignment (and perhaps other open loop contributions to the wavefront error budget) affect the Strehl ratio. We are looking at a number of factors which should improve VOLT performance: 1) The Aluminum mirrors in the DAO 1.2m optical train will be replaced in summer 2008 by Silver mirrors which, along with a re-coated primary, would substantially increase the telescope throughput. 2) We are also considering new open loop controllers which could be used to filter the WFS noise. 3) Finally, we have started looking at using a Gaussian convolution of our subapertures to increase the signal while suppressing particularly the detector pattern noise. Similar in flavor to weighted centroiding[14], we have performed static tests in the lab implementing this approach and at low S/N. We have been able to reduce the WFS noise from 400nm to 270nm. We expect this change should not significantly increase the frame delay or wavefront error due to lag. It will particularly benefit WFS B, which has very large spots and even less light than WFS A. Using this method, we will be able to use WFS B to score the open loop performance at much higher temporal frequencies.

REFERENCES

[1] Hammer, F., et al., "FALCON: a concept to extend adaptive optics corrections to cosmological fields," SPIE, 5382, 727 (2004).

[2] Gavel, D., et al., "Adaptive optics designs for an infrared multi-object spectrograph for TMT," SPIE 6272, 62720R (2006)

[3] Andersen, D. et al., "The MOAO system of the IRMOS near-infrared multi-object spectrograph for TMT," SPIE, 6269, 62694K (2006)

[4] Eikenberry. S., et al., "IRMOS: The near-infrared multi-object spectrograph for TMT," SPIE 6269, 62695W (2006).

[5] Primmerman, C.A., Murphy, D.V., Page, D.A., Zollars, B.G., Barclay, H.T., "Compensation of atmospheric optical distortion using a synthetic beacon," Nature, 353, 141 (1991)

[6] Ammons, S.M., Gavel, D.T., Reinig, M.R., Dillon, D.R., Morzinski, K.M., "On-sky demonstrations of open-loop Shack-Hartmann wavefront sensing with villages," Proc. SPIE 7015 (2008)

[7] Gavel, D.T., et al. "Visible light laser guidestar experimental system (Villages): on-sky tests of new technologies for visible wavelength all-sky coverage adaptive optics systems," Proc. SPIE 7015 (2008)

[8] Myers, R.M., et al. "CANARY: the on-sky NGS/LGS MOAO demonstrator for EAGLE," Proc. SPIE 7015 (2008)

[9] Hubert, Z. et al. "CANARY: NGS-based on-sky MOAO prototype on the WHT," Proc. SPIE 7015 (2008)

[10] Vidal, F., et al. "Tomographic tests for MOAO on the SESAME bench," Proc. SPIE 7015 (2008)

[11] Monet, D.G., et al. "The USNO-B catalog," AJ, 125, 984 (2003)

[12] Jolissaint, L., Véran, J.-P., Conan, R., "Analytical modeling of adaptive optics: foundations of the phase spatial power spectrum approach," JOSAA 23, 382 (2006)

[13] M. Carbillet, et al. "CAOS – a numerical simulation tool for astronomical adaptive optics," SPIE 5490, 637 (2004)

[14] Nicole, M., Fusco, T., Rousset, Michau, V., "Improvement of Shack – Hartmann wave-front sensor measurement for extreme adaptive optics," Opt. Let., 29, 2743 (2004)